Gamma-Ray Burst/Supernova Associations: Energy partition and the case of a magnetar central engine

Hou-Jun Lü[1], Lin Lan[1], Bing Zhang[2,1], En-Wei Liang[1], David Alexander Kann[3], Shen-Shi Du[1], and Jun Shen[1]

ABSTRACT

The favored progenitor model for Gamma-ray Bursts (GRBs) with Supernova (SN) association is the core collapse of massive stars. One possible outcome of such a collapse is a rapidly spinning, strongly magnetized neutron star ("magnetar"). We systematically analyze the multi-wavelength data of GRB/SN associations detected by several instruments before 2017 June. Twenty GRB/SN systems have been confirmed via direct spectroscopic evidence or a clear light curve bump, as well as some spectroscopic evidence resembling a GRB-SN. We derive/collect the basic physical parameters of the GRBs and SNe, and look for correlations among these parameters. We find that the peak brightness, ^{56}Ni mass, and explosion energy of SNe associated with GRBs are statistically higher than other Type Ib/c SNe. A statistically significant relation between the peak energy of GRBs and the peak brightness of their associated SNe is confirmed. No significant correlations are found between the GRB energies (either isotropic or beaming-corrected) and the supernova energy. We investigate the energy partition within these systems and find that the beaming-corrected GRB energy of most systems is smaller than the SN energy, with less than 30% of the total energy distributed in the relativistic jet. The total energy of the systems is typically smaller than the maximum available energy of a millisecond magnetar (2×10^{52} erg), especially if aspherical SN explosions are considered. The data are consistent with-though not proof of-the hypothesis that most, but not all, GRB/SN systems are powered by millisecond magnetars.

Subject headings: gamma rays: general- methods: statistical- radiation mechanisms: non-thermal

[1]Guangxi Key Laboratory for Relativistic Astrophysics, Department of Physics, Guangxi University, Nanning 530004, China; lhj@gxu.edu.cn

[2]Department of Physics and Astronomy, University of Nevada Las Vegas, Las Vegas, NV 89154, USA; zhang@physics.unlv.edu

[3]Instituto de Astrofísica de Andalucía (IAA-CSIC), Glorieta de la Astronomía s/n, E-18008 Granada, Spain

1. Introduction

Gamma-ray bursts (GRBs) and supernovae (SNe) are known as the brightest and most powerful explosions in the universe, with a typical isotropic emission energy of $\sim 10^{52}$ and $\sim 10^{51}$ erg, respectively (Woosley & Bloom 2006; Hjorth & Bloom 2012; Kumar & Zhang 2015; Cano et al. 2017b). Despite the similarity in the released energy between these two types of phenomena, a direct connection between them was not established until the discovery of the first association between an under-luminous GRB 980425 and a Type Ic SN 1998bw at redshift $z = 0.0085$ (Galama et al. 1998; Kippen et al. 1998; Pian et al. 1998; Sadler et al. 1998). A handful of long GRBs associated with spectroscopically identified SNe were henceforth detected, e.g., GRB 030329A/SN 2003dh (Hjorth et al. 2003; Stanek et al. 2003; Kovacevic et al. 2014). More generally, long GRBs typically occur in active star-forming regions in irregular star forming galaxies (Fruchter et al. 2006). All these suggest a direct connection between long GRBs and a special type of Type Ic SNe, both of which are related to the collapse of a special type of massive stars (likely the so-called Wolf-Rayet stars) known as the "collapsars" (e.g., Woosley 1993; Paczyński 1998; Woosley & Bloom 2006; Cano et al. 2017b).

In general, asymmetric stellar explosions invoke a central engine to power the supernova and possibly a GRB (e.g., Bisnovatyi-Kogan 1970). Two types of post-collapse central engine models have been discussed in the literature for these explosions (e.g., Kumar & Zhang 2015, Zhang 2018 for a review): one invoking a stellar-mass black hole fed by an accretion disk (e.g., Popham et al. 1999; Narayan et al. 2001; Lei et al. 2009; van Putten et al. 2011; Liu et al. 2017), and the other invoking a rapidly spinning, strongly magnetized neutron star called a magnetar (Usov 1992; Thompson 1994; Dai & Lu 1998a,b; Wheeler et al. 2000; Zhang & Mészáros 2001; Metzger et al. 2011; Bucciantini et al. 2012; Lü & Zhang 2014).

From the observational point of view, evidence for a magnetar central engine has been collected in both GRBs and SNe. In the *Swift* era, a good fraction of both long and short GRBs exhibit an X-ray plateau followed by a very sharp drop with a temporal decay slope steeper than three, which is known as an internal plateau. This feature is difficult to interpret by the external shock model or by the models invoking a black hole central engine, but it is consistent with the internal dissipation of a long-lasting jet launched by a spinning-down magnetar, which collapses into a black hole at the end of the plateau (e.g., Troja et al. 2007; Lyons et al. 2010; Rowlinson et al. 2010, 2013; Lü & Zhang 2014; Lü et al. 2015; De Pasquale et al. 2016a). On the other hand, the so-called super-luminous SNe (SLSNe), which have a luminosity tens of times higher than normal core-collapse supernovae, are now being routinely detected (Quimby et al. 2007; Gal-Yam 2012; Nicholl et al. 2015). At least some of them require additional energy injection to power the SN emission (Quimby et al.

2011; Nicholl et al. 2014; Wang et al. 2015). The magnetar model is a viable possibility to explain these events by providing the rotational energy via magnetic dipole radiation[1] (e.g., Kasen & Bildsten 2010; Woosley 2010; Dessart et al. 2012; Nicholl et al. 2014; Vreeswijk et al. 2014; Metzger et al. 2015; Wang et al. 2015, 2016; Yu et al. 2017). Mazzali et al. (2014) noticed that the kinetic energy of SNe associated with GRBs tends to cluster near 10^{52} erg, which is below the maximum magnetar spin energy. They then suggested that GRB-SNe may be powered by underlying magnetars.

In any case, magnetars are likely operating in at least some super-luminous SNe and GRBs. One therefore has the following questions. Is it common to have magnetars power GRBs in general, and in particular SN-associated GRBs? What is the energy partition in these events between the relativistic jet (prompt and afterglow emission of the GRB) and the more isotropic emission (SN)? Are there correlations between parameters related to GRBs and SNe?

This paper aims to address these interesting questions through a systematic analysis of a sample of SN-GRB associations. The criteria for sample selection and the performed data analysis are presented in Section 2. Section 3 shows some statistical comparisons of the physical properties of GRBs and SNe and their correlations. The case of a magnetar central engine and the energy partition between GRB and SN in our sample are studied in Section 4. The conclusions are drawn in Section 5 with some discussions. Throughout the paper, a concordance cosmology with parameters $H_0 = 71$ km s^{-1} Mpc $^{-1}$, $\Omega_M = 0.30$, and $\Omega_\Lambda = 0.70$ is adopted to calculate the energetics of GRBs and SNe.

2. Sample selection and data analysis

We extensively searched for the claimed GRB/SN associations before 2017 June from the literature. The criteria of sample selection is that either the associated SN must be confirmed via spectroscopic evidence (SN spectral features in the optical band), or a clear light curve bump is observed at late times in the GRB afterglow emission, and in the meantime a SN is observed independent at the same location with spectroscopic evidence resembling a GRB/SN. To remove ambiguity, we do not include those cases with a bump in the optical afterglow without spectroscopic support. Our entire sample includes 20 GRB/SN events.

[1]Some suggested SLSNe, e.g., the most luminous one (ASASSN-15lh or SN 2015L; Dong et al. 2016) claimed so far, have been also explained in terms of models other than the magnetar model, e.g., tidal disruption events on to a Kerr black hole (Leloudas et al. 2016; Krühler et al. 2018) or the spin-down of a stellar Kerr black hole (van Putten & Della Valle 2017).

Figure 1 shows the X-ray and optical light curves of these GRBs in the rest frame[2]. The redshift (determined from the spectral lines of the host galaxies) and the GRB emission properties are collected from the literature and presented in Table 1.

The properties of the associated SNe are presented in Table 2. The type of the GRB-associated SN is mostly Type Ic except GRB 111209A/SN 2011kl, which was identified as a super-luminous SN (Greiner et al. 2015; Kann et al. 2016; see Table 2). A special X-Ray Outburst (XRO) 080109 (a type of cosmological X-ray transient due to SN shock breakout with a luminosity much lower than GRBs) is also included in our sample, which is associated with a Type Ib SN 2008D (Soderberg et al. 2008).

3. Statistical Properties of GRB/SN events and their Possible Correlations

Our purpose is to compare the observed properties of our GRB/SN associations sample with other typical long GRBs and Type Ib/c SNe, and find out the differences and similarities between them.

3.1. Physical parameters of GRBs

The isotropic prompt γ-ray emission energy ($E_{\gamma,\rm iso}$) of GRBs is usually derived from the observed fluence (S_γ) in the detector's energy band, and extrapolated to the rest-frame 1-10^4 keV using spectral parameters. It is given by

$$\begin{aligned} E_{\gamma,\rm iso} &= 4\pi k D_L^2 S_\gamma (1+z)^{-1} \\ &= 1.3\times10^{51}\ {\rm erg}\ k D_{L,28}^2 (1+z)^{-1} S_{\gamma,-6}, \end{aligned} \quad (1)$$

where z is the redshift, $D_L = 10^{28}$ cm $D_{L,28}$ is the luminosity distance, and k is the k-correction factor from the observed band to 1-10^4 keV in the rest frame (e.g., Bloom et al. 2001; Lü et al. 2014). The convention $Q = 10^x Q_x$ is adopted in cgs units for all parameters throughout this paper. As the spectra of most GRBs in our sample can be modeled with the so-called "Band function" (Band et al. 1993) or the cutoff power-law model, the peak energy of spectrum ($E_{\rm p}$) can be measured from the data. Here, we do not analyze the spectra of GRBs systematically by ourselves, but collect the $E_{\rm p}$ values from the published papers. The $E_{\gamma,\rm iso}$ of GRBs are reported in Table 3.

[2]The X-ray afterglow data of GRBs 011121, 021211, 031203, 130215A, and 140606B are missing due to observational constraints, so they are not presented in the figure.

Another important parameter is the isotropic kinetic energy $E_{\rm K,iso}$, which is measured from the afterglow flux if the normal decay segment of the X-ray or optical afterglow can be observed. This is because this value becomes constant during the normal decay phase (after energy injection during the prior shallow decay phase, Nousek et al. 2006; Zhang et al. 2006). Following the method discussed in Zhang et al. (2007), we calculate $E_{\rm K,iso}$ based on the normal decay phase using the X-ray or optical data. We use the "closure relation"[3] to judge the spectral regime and the profile of the circumburst medium, i.e., (1) $\nu_m < \nu < \nu_c$ for the interstellar medium (ISM) model; (2) $\nu_m < \nu < \nu_c$ for the Wind model; and (3) $\nu > \max(\nu_m, \nu_c)$ for both the ISM and Wind model (in this case, the $E_{\rm K,iso}$ expression does not depend on the medium density, Zhang et al. 2007; Lü & Zhang 2014). These derivations depend on the unknown shock equipartition parameters for electrons (ϵ_e) and for magnetic fields (ϵ_B). In our calculations, we assume $\epsilon_{\rm e} = [0.01 - 0.1]$ and $\epsilon_{\rm B} = [10^{-4} - 10^{-2}]$, which are consistent with the typical values derived in previous studies (e.g., Panaitescu & Kumar 2002; Yost et al. 2003). The Compton parameter is assigned to a typical value $Y = 1$. The $E_{\rm K,iso}$ of GRBs are reported in Table 3.

With the derived $E_{\gamma,\rm iso}$ and $E_{\rm K,iso}$, one can define the total isotropic GRB energy

$$E_{\rm GRB,iso} = E_{\gamma,\rm iso} + E_{\rm K,iso}. \tag{2}$$

To study the true energetics of the GRBs, the jet collimation angle θ_j needs to be derived. We derive this parameter using the time when a steepening break known as the "jet break" is observed in the afterglow light curve. If such a break is not observed, we use the last observational time as the lower limit of the jet-break time. The jet angle information was searched from the literature before (Liang et al. 2008; Lu et al. 2012; the references in Table 1), which is adopted in our analysis. The jet opening angle is derived by using (Frail et al. 2001; Zhang 2018)

$$\begin{aligned} \theta_j &= 0.063 \left(\frac{t_j}{1\ {\rm day}}\right)^{3/8} \left(\frac{1+z}{2}\right)^{-3/8} \left(\frac{\eta_\gamma}{0.2}\right)^{1/8} \\ &\times \left(\frac{E_{\gamma,\rm iso}}{10^{53}\ {\rm erg}}\right)^{-1/8} \left(\frac{n}{0.1\ {\rm cm^{-3}}}\right)^{1/8}, \end{aligned} \tag{3}$$

where t_j is the jet-break time (for non-detections, the last observational time is adopted to infer the lower limit of the jet opening angle), and η_γ is an efficiency conversion factor

[3]This is the relation between temporal α and spectral β index (Zhang & Mészáros 2004; Zhang et al. 2006; Gao et al. 2013).

($\eta_\gamma \equiv E_{\gamma,\rm iso}/E_{\rm K,iso}$). With the derived θ_j, we correct the isotropic values of various forms of energy by multiplying the values of the beaming fraction (Frail et al. 2001)

$$f_b = 1 - \cos\theta_j \simeq (1/2)\theta_j^2, \tag{4}$$

so that $E_\gamma = E_{\gamma,\rm iso} f_b$, and $E_{\rm K} = E_{\rm K,iso} f_b$. We denote $E_{\rm GRB}$ as the total energy of a GRB, which is defined as

$$E_{\rm GRB} = E_\gamma + E_{\rm K} = E_{\rm GRB,iso} f_b, \tag{5}$$

These are reported in Table 3.

The $E_{\gamma,\rm iso}$, $E_{\rm p}$, $E_{\rm K,iso}$ and $\theta_{\rm j}$ (or lower limit) of the GRBs in our sample are summarized in Table 1. Figure 2 presents the distributions of the γ-ray energy and kinetic energy for the isotropic and beaming-corrected values, respectively. With Gaussian fitting, the mean values of the isotropic energies are derived as $\log {\rm E}_{\gamma,\rm iso} = 52.52\pm0.13$ erg and $\log {\rm E}_{\rm K,iso} = 53.35\pm0.13$ erg, respectively. Due to the lack of jet-break detections in some GRBs of our sample, we could only plot the distributions of the beaming-corrected γ-ray and kinetic energies using some of the lower limits, so that no reliable Gaussian distributions can be derived.

3.2. Physical parameters of SNe

When identified, the peak luminosity and peak time of a SN associated with a GRB can be directly inferred from the data. The nickel mass, explosion energy, and ejecta mass of a SN can be estimated from bolometric light curves and spectral properties of the SN. These parameters can provide important clues to understand the progenitors of the SN.

The bolometric light curve data of a SNe are collected from the literature. We apply the analytical model of Arnett (1982) to derive the nickel mass and the ejecta mass. According to this model, the luminosity of SN as a function of time reads

$$\begin{aligned} L(t) &= M_{Ni} \times \exp(-t^2/\tau^2) \\ &\times \{\epsilon_{Ni} \int_0^{t/\tau} A(x)dx + \epsilon_{Co} \int_0^{t/\tau} (B(x) - A(x))dx\} \end{aligned} \tag{6}$$

where

$$\begin{cases} A(x) = 2x \cdot \exp(-2xy + 2xs + x^2), \\ B(x) = 2x \cdot \exp(-2xy + x^2), \\ {\rm y} = \frac{\tau}{2\tau_{\rm Ni}}, \\ {\rm s} = \frac{\tau(\tau_{\rm Co} - \tau_{\rm Ni})}{2\tau_{\rm Co}\tau_{\rm Ni}}, \end{cases} , \tag{7}$$

with $\epsilon_{Ni} = 3.9 \times 10^{10}$ erg s^{-1}g^{-1}, $\epsilon_{Co} = 6.78 \times 10^{9}$ erg s^{-1}g^{-1} (Sutherland & Wheeler 1984; Cappellaro et al. 1997), and the decay life time of ^{56}Ni and ^{56}Co are $\tau_{\rm Ni} = 8.88$ days and $\tau_{\rm Co} = 111.3$ days (Taubenberger et al. 2006), respectively. Here, τ is the effective diffusion time that is related to the opacity (κ), the ejecta mass ($M_{\rm ej}$), as well as the photospheric velocity ($v_{\rm ph}$) that can be determined by the width of the bolometric light curve, which reads

$$\tau \approx \left(\frac{\kappa \cdot M_{\rm ej}}{\beta c \cdot v_{\rm ph}}\right)^{1/2}. \quad (8)$$

where β is a constant of integration (Arnett 1982), c is the speed of light, and the opacity has an assumed typical value $\kappa = 0.07$ cm^{2}g^{-1} (Chugai 2000). We collect the $v_{\rm ph}$ and $M_{\rm ej}$ values from the literature and derive $M_{\rm Ni}$ based on light curve fitting. The kinetic energy of the ejecta is derived as

$$E_{\rm SN} = \frac{1}{2} M_{\rm ej} v_{\rm ph}^2, \quad (9)$$

where we have assumed that the explosion is spherically symmetric. If one assumes that the SN explosion is asymmetric and it is brighter near the polar region (i.e., the GRB jet direction), then the true kinetic energy may be smaller by a factor of a few (e.g., from 2 to 5, Mazzali et al. 2014). Notice that there are five SNe (SNe 2001ke, 2002lt, 2005nc, 2013ez, and 2013fu) that do not have enough data (their SN signature was inferred from the optical bump in the late afterglow light curve). The parameters of those cases are taken from the literature. All together, the derived SN parameters are summarized in Table 2 and 3.

Figure 3 shows a comparison of the bolometric light curves (a) and peak magnitudes (b) of the GRB-associated SNe in our sample and other Type Ib/c SNe (Lyman et al. 2016). The bolometric light curves of the SNe (Figure 3(a)) are plotted with the zero time set at the peak time. For comparison, we plot the bolometric light curves of other Type Ib/c SNe (taken from Lyman et al. 2016) in gray. Figure 3(b) shows the distribution of the peak magnitude of GRB-associated SNe (solid histogram) and that of other Type Ib/c (gray histogram). It can be seen that GRB-associated SNe are systematically brighter than other Type Ib/c SNe. However, a K-S test shows that it is only somewhat unlikely that the offset between the two distributions stems from random chance ($p_{K-S} = 0.1$). Typically, p=0.01 is seen as reasonable, and only p <0.001 is seen as strong evidence for two truly different distributions.

3.3. Statistical correlations of the GRB/SN parameters

To investigate possible relations between GRB parameters and SN parameters, we present a series of scatter plots.

We first investigate how the GRB spectral peak energy, E_p is related to other parameters (e.g., $E_{p,i} - E_{iso}$, $E_p - M_{\rm peak}$, $E_p - t_{\rm peak}$, and $E_p - M_{\rm Ni}$). Figure 4 (a) presents the well-known $E_{\gamma,\rm iso} - E_{\rm p,i}$ correlation (i.e., the so-called Amati relation). Here, $E_{\rm p,i} = E_p(1+z)$ is the cosmological rest-frame peak energy of the GRB. The data of typical long GRBs are taken from Amati et al. (2002) and Zhang et al. (2009). Most GRBs in our sample fall into the 2σ deviation region of the best-fit power-law model for typical long GRBs, and some outliers (including the low-luminosity GRBs 980425, 031203, 140606B, and 161219B and the ultra-long GRB 111209A) are identified. These deviations may be intrinsic, but it is also possible that they are due to an observational bias caused by the lack of detection of soft X-ray emission associated with these GRBs (see e.g., Martone et al. 2017).

Next, we investigate the relation between E_p and the supernova peak bolometric magnitude ($M_{\rm peak}$). Li (2006) discovered a correlation between the two parameters using four pairs of GRB/SN associations and found $E_p \propto M_{\rm peak}^{-1.987}$. We investigate this correlation using our much-expanded sample and find that the correlation still exists, even though the slope is somewhat shallower than the one found in Li (2006). The data and the best-fit correlation are shown in Figure 4 (b). Our best-fit correlation gives

$$\log\ E_p = (-1.36 \pm 0.14) M_{\rm peak} - (23.82 \pm 2.53), \tag{10}$$

with the Pearson linear correlation coefficient $r = 0.92$, corresponding to a probability $P = 0.06$ for zero correlation. This indicates that the $M_{\rm peak}$ and $E_{\rm p}$ are strongly correlated. Cano (2014) suggested a correlation between the brightness and width of the light curves of SNe associated with GRBs as a Pearson's correlation coefficient is $r \sim 0.93$, which may be used as a standardizable candles. As the $E_{\rm p} - M_{\rm peak}$ correlation has a similar r value with that of Cano (2014), it may be used as a potential standard candle as well.

In Figure 4 (c), we plot $E_{\rm p}$ against $M_{\rm Ni}$, the mass of ^{56}Ni. We find that $E_{\rm p}$ is also correlated with $M_{\rm Ni}$ with a large systematic error, i.e.,

$$\log\ {\rm E_p} = (2.65 \pm 0.65) \log\ {\rm M_{Ni}} + (2.81 \pm 0.27), \tag{11}$$

with a Pearson's linear correlation coefficient $r = 0.77$, corresponding to a probability $P = 0.23$ for zero correlation. In Figure 4 (d), we plot E_p against $t_{\rm peak}$. No significant trend is found.

As $E_{\gamma,\rm iso}$ is strongly related to E_p (Amati relation, Fig.4 (a)), we plot $E_{\gamma,\rm iso}$ (or beaming-corrected γ-ray energy E_γ) against $M_{\rm peak}$, $t_{\rm peak}$, and $M_{\rm Ni}$ in Fig. 5. No significant correlations between them are observed. In Fig. 6, we also plot the the total GRB energy ($E_{\rm GRB,iso}$ and $E_{\rm GRB}$) against the three parameters. Again, no significant correlations are observed.

We also investigate some possible correlations among SN parameters. Figure 7(a) shows $M_{\rm peak}$ as a function of $t_{\rm peak}$ for SNe in our sample. No apparent correlation is seen. Figure

7(b) shows $M_{\rm peak}$ against $E_{\rm SN}$ for our sample and other Type Ib/c SNe without associated GRBs. A rough trend of correlation is seen, but statistically no significant correlation can be claimed. Figure 7(c) shows a strong correlation between $M_{\rm peak}$ and $M_{\rm Ni}$, which reads

$$\log {\rm M_{Ni}} = (-0.36 \pm 0.14){\rm M_{peak}} - (7.16 \pm 0.61), \tag{12}$$

with the Pearson's linear correlation coefficient of $r = 0.93$, corresponding to a probability $P = 0.07$ for zero correlation. This is readily understandable, as $M_{\rm Ni}$ is derived making use of the peak luminosity.

4. Energy partition between GRB and SN, and the case of a magnetar central engine

4.1. Energy partition

Figure 8 shows $E_{\rm GRB,iso}$ vs. $E_{\rm SN}$ and $E_{\rm GRB}$ vs. $E_{\rm SN}$ in our sample. The dashed line denotes the equality line. One can see that without beaming correction, $E_{\rm GRB,iso}$ has a wide spread of more than three orders of magnitude. After beaming correction, the distribution of $E_{\rm GRB}$ becomes narrower, now being within two orders of magnitude. There is no direct correlation between the GRB energy and SN energy. In general, the SN energy is greater than the GRB energy. Only the ultra-long GRB 111209A - super-luminous SN 2011kl association shows the opposite trend, i.e., more energy is given to the GRB than the SN.

One can also define the efficiency of GRB/SN events, i.e.,

$$\eta = \frac{E_{\rm GRB}}{E_{\rm GRB} + E_{\rm SN}} \tag{13}$$

to denote the energy partition. Figure 9 shows the distribution of η for our sample. We find that the η is usually less than 0.3 (with the center value ~ 0.1). The GRB 111209A/SN 2011kl system has η greater than 70% (see Table 3).

4.2. The case of a magnetar central engine

The remnant of massive-star core-collapse that produces a GRB is thought to be either a black hole or a rapidly rotating magnetar. The SN is believed to be usually powered by the decay of ^{56}Ni (Maeda & Tominaga 2009). However, the existence of a magnetar as the central engine can inject additional energy to power the SN, making it brighter (e.g.,

Bucciantini et al. 2009; Thompson et al. 2010; Woosley 2010; Metzger et al. 2011; Dessart et al. 2012; Wang et al. 2015, 2016).

A magnetar engine has two specific predictions. First, due to significant energy injection, the SN is expected to be brighter than a normal SN; the latter has a neutron-star engine with a much less spin energy than a millisecond magnetar. This is supported by our data (see Fig.3(b)). The second prediction is that the total energy budget of the system (including both the GRB and the SN) should not exceed the maximum spin energy of the millisecond magnetar, which is $\mathrm{E_{rot}} \sim 2 \times 10^{52}$ erg for a magnetar with $M_{\rm NS} \sim 1.4 M_\odot$ and initial spin period $P_0 \sim 1$ ms. To test this prediction, in Figure 10, we plot the total isotropic GRB energy ($E_{\rm GRB,iso}$), total beaming-corrected GRB energy ($E_{\rm GRB}$), the SN energy ($E_{\rm SN}$), as well as the total explosion energy of the GRB/SN system ($E_{\rm tot} = E_{\rm GRB} + E_{\rm SN}$) as a function of the rest-frame GRB duration $T_{90}/(1+z)$. One can see that the majority of systems have a total energy below the maximum energy budget of a millisecond magnetar. This can be also see in Figure 8, where the maximum energy budget lines are also plotted for $E_{\rm GRB}$ and $E_{\rm SN}$, respectively.

Note that the SN energy $E_{\rm SN}$ is calculated by assuming a spherical symmetry for the explosion. We find that $E_{\rm SN}$ of most SNe are below or close to the maximum rotation energy of magnetar, except in three cases (GRB 021211/SN 2002lt, GRB 130427A/SN 2013cq, and GRB 161219B/SN 2016jca) that exceed this upper limit. In particular, the lack of a jet break 2.5 years after the burst trigger in GRB 130427A (De Pasquale et al. 2016b) indeed poses a challenge to the total energy budget of this event (a structured jet may somewhat alleviate this problem). In these cases, a different central engine, likely a hyper-accreting black hole, might be involved. However, from the distribution of elements (e.g., iron or oxygen) through nebular emission lines, Mazzali et al. (2001) developed 2D explosion models and 3D radiation transport calculations (Maeda et al. 2002; Tanaka et al. 2007), which suggested that SNe are likely aspherical. The derived $E_{\rm SN}$ is likely overestimated, and the real $E_{\rm SN}$ may be smaller by a factor of (2-5) (Mazzali et al. 2014). If we recalculated $E_{\rm SN}$ by reducing the isotropic value by a factor of three, we find that the $E_{\rm SN}$ values of all the systems are roughly in the range of $(0.2-2) \times 10^{52}$ erg (see Figure 10(b)), and the total energy of most GRB/SN system are below the energy budget of a magnetar (see Figure 10(c)). Overall, the data are consistent with-even though not a proof of-the hypothesis that all GRB/SN systems have a magnetar central engine. This conclusion is consistent with that of Mazzali et al. (2014).

5. Conclusions and Discussion

To understand the origin of GRB/SN systems, we systematically study a sample of 20 GRB/SN association systems with robust spectroscopic evidence of the associated SNe. For comparison, we also include other typical long GRBs without observed SN association (Amati et al. 2002; Zhang et al. 2009) and other Type Ib/c SNe without associated GRBs (Lyman et al. 2016). By deriving/collecting basic physical parameters of GRBs and SNe and analyzing their correlations, we are able to reach several interesting conclusions.

- The peak brightness, ^{56}Ni mass and explosion energy of the SNe in our sample are systematically higher than other Type Ib/c SNe without associated GRBs with a K-S test value $p_{KS} = 0.1$. This hints that an additional energy source other than ^{56}Ni decay might be playing the role to power the SNe.

- The beaming-corrected GRB γ-ray energy E_γ and kinetic energy $E_{\rm K}$ in our sample are both less than the maximum available energy of a millisecond magnetar. The SN energy $E_{\rm SN}$ of most systems is also smaller than this energy budget. When aspherical explosions are assumed, most SNe in our sample are below the energy budget limit of a magnetar. The total GRB+SN energy of most systems in our sample are below or close to the maximum rotation energy of a magnetar when assuming aspherical SN explosions, with the SN energy distributed in the range $(0.2-2)\times10^{52}$ erg. All these are consistent (but not a proof) of the hypothesis that most, if not all, GRB/SN systems are powered by millisecond magnetars. Indeed, a few hyper-energetic GRB/SN events are identified, which may require a hyper-accreting black hole as the central engine.

- The energy partition between GRB and SN in these systems is such that most of the energy is carried by the SN. The GRB energy is typically less than 30%, with a center value of about 10% of the total budget.

- Several interesting statements may be made regarding some correlations. First, even though most systems in our sample satisfy the so-called Amati relation ($E_{\gamma,\rm iso} - E_{\rm p,i}$, Amati et al. 2002), there are apparent outliers in the GRB/SN systems to this relation. A tentative relation between $E_{\rm p}$ and $M_{\rm peak}$ (Li 2006) is confirmed in our study.

Some famous GRB/SN associations (e.g,. GRB 980425/SN 1998bw and GRB 060218/SN 2006aj) belong to the so-called low-luminosity GRBs (e.g., Campana et al. 2006; Liang et al. 2007; Soderberg et al. 2008; Virgili et al. 2009). Some authors suggested that these systems may be related to shock breakouts (e.g., Li 2007; Wang & Mészáros 2007; Chevalier & Fransson 2008; Bromberg et al. 2011; Nakar & Sari 2012). These bursts typically have

smooth, long-duration burst light curves and low luminosities. Successful jets typically have variable light curves and high luminosities. The separation line between the two types of GRBs is $\sim 10^{48}$ erg s^{-1} (Zhang et al. 2012). In Figure 11, we plot the GRB luminosity against duration in our sample. It is interesting to see that only four systems in our sample are below the low-luminosity GRB category defined by Zhang et al. (2012). Most other GRBs in our sample are actually high-luminosity GRBs. The similarity of the SN properties between low-luminosity and high-luminosity GRBs suggests that they likely share a similar type of the progenitor star, with the difference in the GRB emission properties defined by some parameters related to jet launching (e.g., jet power, engine duration).

Besides serving as central engines in GRB/SN systems, young magnetars have been invoked to power other systems as well, including super-luminous supernovae (e.g., Kasen & Bildsten 2010; Woosley 2010; Wang et al. 2015, 2016; Dong et al. 2016), NS-NS mergers (Dai et al. 2006; Fan & Xu 2006; Metzger et al. 2008; Rowlinson et al. 2010, 2013; Gao et al. 2013a; Yu et al. 2013; Zhang 2013; Metzger & Piro 2014; Lü et al. 2015; Gao et al. 2016), and even fast radio bursts (Zhang 2014; Murase et al. 2016; Metzger et al. 2017). The different properties of these transient events may be related to different parameters of the underlying magnetars (Metzger et al. 2015; Yu et al. 2017).

We thank J. D. Lyman for sharing the Type Ib/c SNe data with us, Wei-Hua Lei for helpful discussion, and the anonymous referee for helpful comments. D.A.K acknowledges financial support from the Spanish research project AYA 2014-58381-P, and from Juan de la Cierva Incorporación fellowship IJCI-2015-26153. This work is supported by the National Basic Research Program (973 Programme) of China 2014CB845800, the National Natural Science Foundation of China (grant Nos.11603006, 11851304, 11533003, and U1731239), Guangxi Science Foundation (grant Nos. 2017GXNSFFA198008, 2016GXNSFCB380005, 2015GXNSFDA39002, and AD17129006), the One-Hundred-Talents Program of Guangxi colleges, the high-level innovation team and outstanding scholar program in Guangxi colleges, Scientific Research Foundation of Guangxi University (grant No. XGZ150299), and special funding for Guangxi distinguished professors (Bagui Yingcai & Bagui Xuezhe).

REFERENCES

Ackermann, M., Ajello, M., Asano, K., et al. 2014, Science, 343, 42

Amati, L., Frontera, F., Tavani, M., et al. 2002, A&A, 390, 81

Arnett, W. D. 1982, ApJ, 253, 785

Ashall, C., Pian, E., Mazzali, P. A., et al. 2017, arXiv:1702.04339

Band, D., Matteson, J., Ford, L., et al. 1993, ApJ, 413, 281

Berger, E., Chornock, R., Holmes, T. R., et al. 2011, ApJ, 743, 204

Bisnovatyi-Kogan, G. S. 1970, AZh, 47, 813

Bloom, J. S., Frail, D. A., & Sari, R. 2001, AJ, 121, 2879

Bromberg, O., Nakar, E., & Piran, T. 2011, ApJ, 739, L55

Bucciantini, N., Metzger, B. D., Thompson, T. A., & Quataert, E. 2012, MNRAS, 419, 1537

Bucciantini, N., Quataert, E., Metzger, B. D., et al. 2009, MNRAS, 396, 2038

Bufano, F., Pian, E., Sollerman, J., et al. 2012, ApJ, 753, 67

Campana, S., Mangano, V., Blustin, A. J., et al. 2006, Nature, 442, 1008

Cano, Z. 2014, ApJ, 794, 121

Cano, Z., de Ugarte Postigo, A., Perley, D., et al. 2015, MNRAS, 452, 1535

Cano, Z., de Ugarte Postigo, A., Pozanenko, A., et al. 2014, A&A, 568, A19

Cano, Z., Izzo, L., de Ugarte Postigo, A., et al. 2017a, A&A, 605, A107

Cano, Z., Wang, S.-Q., Dai, Z.-G., & Wu, X.-F. 2017b, Advances in Astronomy, 2017, 8929054

Cappellaro, E., Mazzali, P. A., Benetti, S., et al. 1997, A&A, 328, 203

Chevalier, R. A., & Fransson, C. 2008, ApJ, 683, L135

Chugai, N. N. 2000, Astronomy Letters, 26, 797

Clocchiatti, A., Suntzeff, N. B., Covarrubias, R., & Candia, P. 2011, AJ, 141, 163

Cobb, B. E., Bloom, J. S., Perley, D. A., et al. 2010, ApJ, 718, L150

Dai, Z. G., & Lu, T. 1998a, Physical Review Letters, 81, 4301

Dai, Z. G., & Lu, T. 1998b, A&A, 333, L87

Dai, Z. G., Wang, X. Y., Wu, X. F., & Zhang, B. 2006, Science, 311, 1127

D'Elia, V., Pian, E., Melandri, A., et al. 2015, A&A, 577, A116

De Pasquale, M., Oates, S. R., Racusin, J. L., et al. 2016a, MNRAS, 455, 1027

De Pasquale, M., Page, M. J., Kann, D. A., et al. 2016b, MNRAS, 462, 1111

Della Valle, M., Malesani, D., Benetti, S., et al. 2003, A&A, 406, L33

Della Valle, M., Malesani, D., Bloom, J. S., et al. 2006, ApJ, 642, L103

Deng, J., Tominaga, N., Mazzali, P. A., Maeda, K., & Nomoto, K. 2005, ApJ, 624, 898

Dessart, L., Hillier, D. J., Waldman, R., Livne, E., & Blondin, S. 2012, MNRAS, 426, L76

Dong, S., Shappee, B. J., Prieto, J. L., et al. 2016, Science, 351, 257

Fan, Y.-Z., & Xu, D. 2006, MNRAS, 372, L19

Fan, Y.-Z., Zhang, B.-B., Xu, D., Liang, E.-W., & Zhang, B. 2011, ApJ, 726, 32

Ferrero, P., Kann, D. A., Zeh, A., et al. 2006, A&A, 457, 857

Frail, D. A., Kulkarni, S. R., Sari, R., et al. 2001, ApJ, 562, L55

Fruchter, A. S., Levan, A. J., Strolger, L., et al. 2006, Nature, 441, 463

Gal-Yam, A., Moon, D.-S., Fox, D. B., et al. 2004, ApJ, 609, L59

Gal-Yam, A. 2012, Science, 337, 927

Galama, T. J., Vreeswijk, P. M., van Paradijs, J., et al. 1998, Nature, 395, 670

Gao, H., Lei, W.-H., Zou, Y.-C., Wu, X.-F., & Zhang, B. 2013a, NewAR, 57, 141

Gao, H., Ding, X., Wu, X.-F., Zhang, B., & Dai, Z.-G. 2013b, ApJ, 771, 86

Gao, H., Zhang, B., & Lü, H.-J. 2016, Phys. Rev. D, 93, 044065

Greiner, J., Mazzali, P. A., Kann, D. A., et al. 2015, Nature, 523, 189

Hjorth, J., & Bloom, J. S. 2012, Chapter 9 in "Gamma-Ray Bursts", Cambridge Astrophysics Series 51, eds. C. Kouveliotou, R. A. M. J. Wijers and S. Woosley, Cambridge University Press (Cambridge), p. 169-190, 169

Hjorth, J., Sollerman, J., Møller, P., et al. 2003, Nature, 423, 847

Iwamoto, K. 1999, ApJ, 512, L47

Jin, Z.-P., Covino, S., Della Valle, M., et al. 2013, ApJ, 774, 114

Kann, D. A., Klose, S., Zhang, B., et al. 2010, ApJ, 720, 1513

Kann, D. A., Schady, P., Olivares E., F., et al. 2017, arXiv:1706.00601

Kann, D. A., Schady, P., Olivares E., F., et al. 2016, arXiv:1606.06791

Kasen, D., & Bildsten, L. 2010, ApJ, 717, 245

Kippen, R. M., Briggs, M. S., Kommers, J. M., et al. 1998, ApJ, 506, L27

Kouveliotou, C., Woosley, S. E., Patel, S. K., et al. 2004, ApJ, 608, 872

Kovacevic, M., Izzo, L., Wang, Y., et al. 2014, A&A, 569, A108

Krühler, T., Fraser, M., Leloudas, G., et al. 2018, A&A, 610, A14

Kumar, P., & Zhang, B. 2015, Phys. Rep., 561, 1

Lü, H.-J., & Zhang, B. 2014, ApJ, 785, 74

Lü, H.-J., Zhang, B., Lei, W.-H., Li, Y., & Lasky, P. D. 2015, ApJ, 805, 89

Lü, H.-J., Zhang, B., Liang, E.-W., Zhang, B.-B., & Sakamoto, T. 2014, MNRAS, 442, 1922

Larsson, J., Racusin, J. L., & Burgess, J. M. 2015, ApJ, 800, L34

Lei, W. H., Wang, D. X., Zhang, L., et al. 2009, ApJ, 700, 1970

Leloudas, G., Fraser, M., Stone, N. C., et al. 2016, Nature Astronomy, 1, 0002

Li, L.-X. 2008, MNRAS, 388, 603

Li, L.-X. 2007, MNRAS, 375, 240

Li, L.-X. 2006, MNRAS, 372, 1357

Liang, E.-W., Racusin, J. L., Zhang, B., Zhang, B.-B., & Burrows, D. N. 2008, ApJ, 675, 528-552

Liang, E., Zhang, B., Virgili, F., & Dai, Z. G. 2007, ApJ, 662, 1111

Liu, T., Gu, W.-M., & Zhang, B. 2017, NewAR, 79, 1

Lu, R.-J., Wei, J.-J., Liang, E.-W., et al. 2012, ApJ, 756, 112

Lyman, J. D., Bersier, D., James, P. A., et al. 2016, MNRAS, 457, 328

Lyons, N., O'Brien, P. T., Zhang, B., et al. 2010, MNRAS, 402, 705

Maeda, K., Nakamura, T., Nomoto, K., et al. 2002, ApJ, 565, 405

Maeda, K., & Tominaga, N. 2009, MNRAS, 394, 1317

Martone, R., Izzo, L., Della Valle, M., et al. 2017, A&A, 608, A52

Maselli, A., Melandri, A., Nava, L., et al. 2014, Science, 343, 48

Mazzali, P. A., McFadyen, A. I., Woosley, S. E., Pian, E., & Tanaka, M. 2014, MNRAS, 443, 67

Mazzali, P. A., Deng, J., Pian, E., et al. 2006, ApJ, 645, 1323

Mazzali, P. A., Deng, J., Tominaga, N., et al. 2003, ApJ, 599, L95

Mazzali, P. A., Nomoto, K., Patat, F., & Maeda, K. 2001, ApJ, 559, 1047

Mazzali, P. A., Valenti, S., Della Valle, M., et al. 2008, Science, 321, 1185

Melandri, A., Pian, E., D'Elia, V., et al. 2014, A&A, 567, A29

Melandri, A., Pian, E., Ferrero, P., et al. 2012, A&A, 547, A82

Metzger, B. D., Giannios, D., Thompson, T. A., Bucciantini, N., & Quataert, E. 2011, MNRAS, 413, 2031

Metzger, B. D., Quataert, E., & Thompson, T. A. 2008, MNRAS, 385, 1455

Metzger, B. D., Berger, E., & Margalit, B. 2017, ApJ, 841, 14

Metzger, B. D., Margalit, B., Kasen, D., & Quataert, E. 2015, MNRAS, 454, 3311

Metzger, B. D., & Piro, A. L. 2014, MNRAS, 439, 3916

Mirabal, N., Halpern, J. P., An, D., Thorstensen, J. R., & Terndrup, D. M. 2006, ApJ, 643, L99

Murase, K., Kashiyama, K., & Mészáros, P. 2016, MNRAS, 461, 1498

Nakamura, T., Mazzali, P. A., Nomoto, K., & Iwamoto, K. 2001, ApJ, 550, 991

Nakar, E., & Sari, R. 2012, ApJ, 747, 88

Narayan, R., Piran, T., & Kumar, P. 2001, ApJ, 557, 949

Nicholl, M., Smartt, S. J., Jerkstrand, A., et al. 2014, MNRAS, 444, 2096

Nicholl, M., Smartt, S. J., Jerkstrand, A., et al. 2015, MNRAS, 452, 3869

Nousek, J. A., Kouveliotou, C., Grupe, D., et al. 2006, ApJ, 642, 389

Olivares E., F., Greiner, J., Schady, P., et al. 2015, A&A, 577, A44

Paczyński, B. 1998, Gamma-Ray Bursts, 4th Hunstville Symposium, 428, 783

Panaitescu, A., & Kumar, P. 2002, ApJ, 571, 779

Pian, E., Antonelli, L. A., Piro, L., & Feroci, M. 1998, GRB Coordinates Network, 158, 1

Popham, R., Woosley, S. E., & Fryer, C. 1999, ApJ, 518, 356

Quimby, R. M., Kulkarni, S. R., Kasliwal, M. M., et al. 2011, Nature, 474, 487

Quimby, R. M., Aldering, G., Wheeler, J. C., et al. 2007, ApJ, 668, L99

Rowlinson, A., O'Brien, P. T., Metzger, B. D., Tanvir, N. R., & Levan, A. J. 2013, MNRAS, 430, 1061

Rowlinson, A., O'Brien, P. T., Tanvir, N. R., et al. 2010, MNRAS, 409, 531

Sadler, E. M., Stathakis, R. A., Boyle, B. J., & Ekers, R. D. 1998, IAU Circ., 6901, 1

Schulze, S., Malesani, D., Cucchiara, A., et al. 2014, A&A, 566, A102

Singer, L. P., Cenko, S. B., Kasliwal, M. M., et al. 2013, ApJ, 776, L34

Soderberg, A. M., Berger, E., Page, K. L., et al. 2008, Nature, 453, 469

Sparre, M., Sollerman, J., Fynbo, J. P. U., et al. 2011, ApJ, 735, L24

Stanek, K. Z., Matheson, T., Garnavich, P. M., et al. 2003, ApJ, 591, L17

Sutherland, P. G., & Wheeler, J. C. 1984, ApJ, 280, 282

Tanaka, M., Maeda, K., Mazzali, P. A., & Nomoto, K. 2007, ApJ, 668, L19

Taubenberger, S., Pastorello, A., Mazzali, P. A., et al. 2006, MNRAS, 371, 1459

Thompson, C. 1994, MNRAS, 270, 480

Thompson, T. A., Metzger, B. D., & Bucciantini, N. 2010, American Institute of Physics Conference Series, 1279, 81

Toy, V. L., Cenko, S. B., Silverman, J. M., et al. 2016, ApJ, 818, 79

Troja, E., Cusumano, G., O'Brien, P. T., et al. 2007, ApJ, 665, 599

Tsvetkova, A., Frederiks, D., Golenetskii, S., et al. 2017, ApJ, 850, 161

Usov, V. V. 1992, Nature, 357, 472

van Putten, M. H. P. M., Della Valle, M., & Levinson, A. 2011, A&A, 535, L6

van Putten, M. H. P. M., & Della Valle, M. 2017, MNRAS, 464, 3219

Vergani, S. D., Flores, H., Covino, S., et al. 2011, A&A, 535, A127

Vestrand, W. T., Wren, J. A., Panaitescu, A., et al. 2014, Science, 343, 38

Virgili, F. J., Liang, E.-W., & Zhang, B. 2009, MNRAS, 392, 91

Volnova, A. A., Pruzhinskaya, M. V., Pozanenko, A. S., et al. 2017, MNRAS, 467, 3500

Vreeswijk, P. M., Savaglio, S., Gal-Yam, A., et al. 2014, ApJ, 797, 24

Wang, S. Q., Liu, L. D., Dai, Z. G., Wang, L. J., & Wu, X. F. 2016, ApJ, 828, 87

Wang, S. Q., Wang, L. J., Dai, Z. G., & Wu, X. F. 2015, ApJ, 799, 107

Wang, X.-Y., & Mészáros, P. 2007, ApJ, 670, 1247

Weiler, K. W., Panagia, N., & Montes, M. J. 2001, ApJ, 562, 670

Wheeler, J. C., Yi, I., Höflich, P., & Wang, L. 2000, ApJ, 537, 810

Woosley, S. E. 2010, ApJ, 719, L204

Woosley, S. E. 1993, ApJ, 405, 273

Woosley, S. E., & Bloom, J. S. 2006, ARA&A, 44, 507

Xu, D., de Ugarte Postigo, A., Leloudas, G., et al. 2013, ApJ, 776, 98

Xu, D., Watson, D., Fynbo, J., et al. 2008, 37th COSPAR Scientific Assembly, 37, 3512

Yost, S. A., Harrison, F. A., Sari, R., & Frail, D. A. 2003, ApJ, 597, 459

Yu, Y.-W., Zhang, B., & Gao, H. 2013, ApJ, 776, L40

Yu, Y.-W., Zhu, J.-P., Li, S.-Z., Lü, H.-J., & Zou, Y.-C. 2017, ApJ, 840, 12

Zhang, B.-B., Fan, Y.-Z., Shen, R.-F., et al. 2012, ApJ, 756, 190

Zhang, B. 2013, ApJ, 763, L22

Zhang, B. 2014, ApJ, 780, L21

Zhang, B. 2018, The Physics of Gamma-Ray Bursts, Cambridge University Press, in press

Zhang, B., Fan, Y. Z., Dyks, J., et al. 2006, ApJ, 642, 354

Zhang, B., Liang, E., Page, K. L., et al. 2007, ApJ, 655, 989

Zhang, B., & Mészáros, P. 2004, International Journal of Modern Physics A, 19, 2385

Zhang, B., & Mészáros, P. 2001, ApJ, 552, L35

Zhang, B., Zhang, B.-B., Virgili, F. J., et al. 2009, ApJ, 703, 1696

Table 1. The properties of prompt and afterglow emission of GRBs in our sample.

GRB/SN (Name)	Detectors[a]	Redshift (z)	T_{90} (s)	E_p [b] (keV)	θ_j [c] (Degree)	References
980425/1998bw	*BeppoSAX*	0.0085	35	55±21	11±3	(1)-(3)
011121/2001ke	*BeppoSAX/KW*	0.362	28	819^{+108}_{-96}	4.49±0.16	(4)
021211/2002lt	*HETE-II*	1.006	4	47±5	4.82±0.68	(5)
030329/2003dh	*HETE-II*	0.1685	23	79±3	3.8±0.05	(1),(6)
031203/2003lw	*INTEGRAL*	0.1055	37	159±51	9±2	(1),(7)
050525A/2005nc	*Swift/KW*	0.606	8.8	84±2	2.12±0.46	(8),(9)
060218/2006aj	*Swift*	0.0334	2100	4.9±1.2	12.6±3.95	(1),(10)-(12)
080109/2008d	*Swift*	0.007	600	$0.12^{+0.23}_{-0.089}$	8.09 ↑	(13)-(15)
081007/2008hw	*Swift/Fermi*	0.5295	8	61±15	11.09 ↑	(16),(17)
091127/2009nz	*Swift/KW/Fermi*	0.49	9	36±2	5.5±1.5	(17)-(19)
100316D/2010bh	*Swift*	0.0591	> 1300	18^{+3}_{-2}	5.6 ↑	(1),(20),(21)
101219B/2010ma	*Swift/Fermi*	0.55	51	70±8	9.07 ↑	(17),(22)
111209A/2011kl	*Swift/KW*	0.677	~ 10000	520±89	9.17±1.5	(23)-(25)
120422A/2012bz	*Swift*	0.283	5	33^{+39}_{-33}	23±7	(26)-(28)
130215A/2013ez	*Swift/Fermi*	0.597	66	155±63	10.16 ↑	(29)
130427A/2013cq	*Fermi/Swift*	0.3399	163	830±5	7.5 ↑	(30)-(33)
130702A/2013dx	*Fermi/KW*	0.145	59	10±1	14±4	(34)-(36)
130831A/2013fu	*Swift/KW*	0.479	33	67±4	3.17 ↑	(29)
140606B/iPTF14bfu	*Fermi/KW*	0.384	23	579±135	11.5 ↑	(37)
161219B/2016jca	*Swift/KW*	0.1475	10	93±29	~ 40	(38),(39)

[a]Detected by different instruments: KW is Konus-Wind.

[b]The peak energy in the E^2N(E) spectrum of the prompt emission.

[c]The jet opening angle of GRBs measured from the afterglow. Upward-pointing arrows denote lower limits for the jet opening angles.

References. — (1)Hjorth & Bloom 2012;(2)Iwamoto 1999;(3)Kouveliotou et al. 2004;(4)Tsvetkova et al. 2017;(5)Della Valle et al. 2003;(6)Deng et al. 2005(7)Gal-Yam et al. 2004;(8)Della Valle et al. 2006;(9)Kovacevic et al. 2014;(10)Ferrero et al. 2006;(11)Campana et al. 2006;(12)Mirabal et al. 2006;(13)Xu et al.2008;(14)Li 2008;(15)Soderberg et al. 2008;(16)Jin et al. 2013;(17)Olivares E et al. 2015;(18)Berger et al. 2011;(19)Vergani et al. 2011;(20)Bufano et al. 2012;(21)Fan et al. 2011;(22)Larsson et al. 2015;(23)Greiner et al. 2015;(24)Kann et al. 2016;(25)Kann et al. 2017;(26)Zhang et al. 2012;(27)Melandri et al. 2012;(28)Schulze et al. 2014;(29)Cano et al. 2014;(30)Xu et al.2013;(31)Vestrand et al. 2014;(32)Ackermann et al. 2014;(33)Maselli et al. 2014;(34)Singer et al. 2013;(35)D'Elia et al. 2015;(36)Volnova et al. 2017;(37)Cano et al. 2015;(38)Ashall et al. 2017;(39)Cano et al. 2017a

Table 2. The observational properties and derived parameters of SNe associated with GRBs.

GRB/SN (Name)	SN (Type)	SN[a] (Evidence)	$M_{\rm peak}$[b] (Mag)	$t_{\rm peak}$[b] (Day)	$M_{\rm Ni}$[c] ($M_\odot$)	$M_{\rm ejec}$[d] ($M_\odot$)	References
980425/1998bw	Ic	Spec.	-18.86±0.2	∼ 17	0.54±0.02	6.8±0.57	(1)-(4)
011121/2001ke	Ic	Bump/spec.	-18.55±0.55	13±1	0.35±0.01	4.44±0.82	(5)
021211/2002lt	Ic	Spec.	-18.8±0.4	∼ 14	0.4±0.14	7.16±5.99	(6)
030329/2003dh	Ic	Spec.	-18.79±0.23	11.5±1.5	0.54±0.13	5.06±1.65	(1),(7),(8)
031203/2003lw	Ic	Spec.	-18.92±0.2	21.5±3.5	0.57±0.04	8.22±0.76	(1),(9)
050525A/2005nc	Ic	Spec.	-18.8±0.6	∼ 12	0.42±0.02	4.75±1.08	(10),(11)
060218/2006aj	Ic	Spec.	-18.16±0.1	10±0.5	0.28±0.08	2.58±0.55	(1),(12)-(14)
080109/2008d	Ib	Spec.	-16.9±0.2	19±0.8	0.09±0.01	5.3±1	(15)-(18)
081007/2008hw	Ic	Bump/spec.	-18.5±0.5	12±3	0.39±0.06	2.3±1	(19),(20)
091127/2009nz	Ic	Bump/spec.	-18.65±0.2	15±2	0.33±0.01	4.69±0.13	(20)-(22)
100316D/2010bh	Ic	Spec.	-18.45±0.18	8.48±1.06	0.12±0.02	2.47±0.23	(1),(23)
101219B/2010ma	Ic	Spec.	-18.5±0.25	10±2	0.43±0.03	1.3±0.4	(20),(24)
111209A/2011kl	SLSN	Spec.	-19.8±0.2	14±0.5	1±0.1	3±1	(25)-(27)
120422A/2012bz	Ic	Spec.	-18.56±0.15	16.69±1.28	0.57±0.07	6.1±0.49	(28)-(30)
130215A/2013ez	Ic	Spec.	-18.85±0.15	6.41±0.34	0.375±0.025	—	(31)
130427A/2013cq	Ic	Spec.	-18.91±0.2	∼ 15.2	0.38±0.02	6.27±0.69	(32)-(35)
130702A/2013dx	Ic	Spec.	-18.4±0.4	17.2±0.34	0.38±0.01	3±0.1	(36)-(38)
130831A/2013fu	Ic	Spec.	-18.89±0.05	18.53±0.07	0.48±0.07	6.71±0.2	(31)
140606B/iPTF14bfu	Ic	Spec.	-19.61±0.27	16.32±1.63	0.4±0.2	5±2	(39)
161219B/2016jca	Ic	Spec.	-19.04±0.05	10.7±0.3	0.4±0.1	5.8±0.3	(40),(41)

[a]The evidence of a SN associated with a GRB. "spec." is strong spectroscopic evidence, and "bump" is a clear light curve bump with some spectroscopic evidence.

[b]The peak magnitute and peak time in the SN light curve.

[c]The mass of Nickel measured from the SN.

[d]The mass of ejecta in the blastwave.

References. — (1)Hjorth & Bloom 2012;(2)Weiler et al.2001;(3)Nakamura etal. 2001;(4)Clocchiatti et al. 2011;(5)Tsvetkova et al. 2017;(6)Della Valle et al. 2003;(7)Deng et al. 2005;(8)Mazzali et al. 2003;(9)Mazzali et al. 2006;(10)Della Valle et al. 2006;(11)Kovacevic et al. 2014;(12)Campana et al. 2006;(13)Mirabal et al. 2006;(14)Li 2007;(15)Xu et al. 2008;(16)Mazzali et al.2008;(17)Li 2008;(18)Soderberg et al. 2008;(19)Jin et al. 2013;(20)Olivares E et al. 2015;(21)Berger et al. 2011;(22)Cobb et al. 2010;(23)Bufano et al. 2012;(24)Sparre et al. 2011;(25)Greiner et al. 2015;(26)Kann et al. 2016;(27)Kann et al. 2017;(28)Zhang et al. 2012;(29)Melandri et al. 2012;(30)Schulze et al. 2014;(31)Cano et al. 2014;(32)Xu et al. 2013;(33)Vestrand et al. 2014;(34)Ackermann et al. 2014;(35)Melandri et al. 2014;(36)D'Elia et al. 2015;(37)Toy et al. 2016;(38)Volnova et al. 2017;(39)Cano et al. 2015;(40)Ashall et al. 2017;(41)Cano et al. 2017a

Table 3. The derived energies of of GRBs and SNe in our sample.

GRB/SN (Name)	$E_{\gamma,iso}$ [a] (erg)	E_{γ} [a] (erg)	$E_{K,iso}$ [b] (erg)	E_{K} [b] (erg)	$E_{GRB,iso}$ [c] (erg)	E_{GRB} [c] (erg)	E_{SN} [d] (erg)	$\eta\%$ [e]
980425/1998bw	$(9\pm0.87)\times10^{47}$	$(1.66\pm1.19)\times10^{46}$	$2^{+4.4}_{-0.6}\times10^{49}$	$3.68^{+10.41}_{-1.18}\times10^{47}$	$2.09^{+4.41}_{-0.61}\times10^{49}$	$3.85^{+10.51}_{-3.51}\times10^{47}$	$(1.3\pm0.1)\times10^{52}$	$(2.96\pm1)\times10^{-3}$
011121/2001ke	$(1.02\pm0.15)\times10^{53}$	$(2.25\pm0.32)\times10^{47}$	$5.83^{+12.83}_{-1.3}\times10^{53}$	$2.14^{+4.49}_{-0.54}\times10^{51}$	$6.85^{+12.98}_{-1.45}\times10^{53}$	$2.51^{+5.27}_{-0.63}\times10^{51}$	$(1.77\pm0.88)\times10^{52}$	12.36 ± 3.64
021211/2002lt	$(6.6\pm0.6)\times10^{51}$	$(2.33\pm0.92)\times10^{49}$	$6.62^{+14.58}_{-1.46}\times10^{52}$	$2.34^{+5.86}_{-0.19}\times10^{50}$	$7.28^{+14.61}_{-1.52}\times10^{52}$	$2.57^{+5.93}_{-1.31}\times10^{50}$	$(2.85\pm1.3)\times10^{52}$	0.89 ± 0.45
030329/2003dh	$(1.7\pm0.3)\times10^{52}$	$(3.74\pm3.56)\times10^{49}$	$1.82^{+4.1}_{-0.4}\times10^{52}$	$4^{+14.31}_{-2.44}\times10^{49}$	$3.52^{+4.4}_{-0.7}\times10^{52}$	$7.73^{+2}_{-1.18}\times10^{49}$	$(1.21\pm0.39)\times10^{52}$	0.63 ± 0.27
031203/2003lw	$(9\pm4)\times10^{49}$	$(1.11\pm1.04)\times10^{48}$	$1.44^{+3.16}_{-0.32}\times10^{51}$	$1.77^{+4.77}_{-0.48}\times10^{49}$	$1.53^{+3.2}_{-0.36}\times10^{51}$	$1.89^{+4.88}_{-1.37}\times10^{49}$	$(1.59\pm0.15)\times10^{52}$	0.12 ± 0.35
050525A/2005nc	$(2.39\pm0.15)\times10^{52}$	$(1.57\pm0.76)\times10^{49}$	$4.48^{+9.85}_{-0.98}\times10^{52}$	$3.06^{+8.21}_{-0.81}\times10^{49}$	$6.78^{+9.85}_{-0.98}\times10^{52}$	$4.64^{+8.97}_{-2.9}\times10^{49}$	$(1.89\pm0.75)\times10^{52}$	0.25 ± 0.49
060218/2006aj	$(5.9\pm0.3)\times10^{49}$	$(1.43\pm1.11)\times10^{48}$	$2.67^{+5.88}_{-0.59}\times10^{49}$	$6.45^{+18.9}_{-3.25}\times10^{47}$	$8.57^{+6.18}_{-0.89}\times10^{49}$	$2.07^{+2.99}_{-1.72}\times10^{48}$	$(6.1\pm0.14)\times10^{51}$	0.03 ± 0.05
080109/2008d	$(1.3^{+1.5}_{-0.7})\times10^{46}$	$1.3\times10^{44}\uparrow$	$4.46^{+9.84}_{-0.99}\times10^{48}$	$4.44\times10^{46}\uparrow$	$4.47^{+9.84}_{-0.98}\times10^{48}$	$4.45\times10^{46}\uparrow$	$(6\pm3)\times10^{51}$	$7.42\times10^{-4}\uparrow$
081007/2008hw	$\sim1.5\times10^{51}$	$2.81\times10^{49}\uparrow$	$7.52^{+17.08}_{-1.66}\times10^{52}$	$1.41\times10^{51}\uparrow$	$7.67^{+17.71}_{-1.65}\times10^{52}$	$1.43\times10^{51}\uparrow$	$(9\pm5)\times10^{51}$	$13.7\uparrow$
091127/2009nz	$\sim1.1\times10^{52}$	$(5.06\pm3.14)\times10^{49}$	$3.33^{+7.32}_{-0.74}\times10^{52}$	$1.53^{+4.34}_{-0.61}\times10^{50}$	$4.43^{+7.37}_{-0.73}\times10^{52}$	$2.04^{+4.66}_{-1.6}\times10^{50}$	$(8.1\pm0.2)\times10^{51}$	2.45 ± 5.81
100316D/2010bh	$(6\pm0.3)\times10^{49}$	$2.86\times10^{47}\uparrow$	$5.88^{+12.94}_{-1.3}\times10^{53}$	$2.8\times10^{51}\uparrow$	$5.88^{+12.94}_{-1.3}\times10^{53}$	$2.8\times10^{51}\uparrow$	$(9.2\pm0.8)\times10^{51}$	$23.33\uparrow$
101219B/2010ma	$(4.2\pm0.3)\times10^{51}$	$5.26\times10^{49}\uparrow$	$1.76^{+3.88}_{-0.39}\times10^{53}$	$2.2\times10^{51}\uparrow$	$1.8^{+13.8}_{-0.39}\times10^{53}$	$2.25\times10^{51}\uparrow$	$(1\pm0.6)\times10^{52}$	$18.37\uparrow$
111209A/2011kl	$(5.54\pm0.7)\times10^{53}$	$(7.09\pm3.4)\times10^{51}$	$8^{+17.6}_{-1.76}\times10^{53}$	$1.02^{+2.61}_{-0.14}\times10^{52}$	$1.35^{+1.83}_{-0.25}\times10^{54}$	$1.73^{+2.95}_{-0.93}\times10^{52}$	$(5.5\pm3.5)\times10^{51}$	75.87 ± 16.6
120422A/2012bz	$(2.4\pm0.8)\times10^{50}$	$(1.93\pm1.2)\times10^{49}$	$2.94^{+6.49}_{-0.65}\times10^{52}$	$2.37^{+6.88}_{-1.14}\times10^{51}$	$2.97^{+6.49}_{-0.66}\times10^{52}$	$2.39^{+6.9}_{-2.21}\times10^{51}$	$(1.53\pm0.13)\times10^{52}$	13.5 ± 14.3
130215A/2013ez	$(3.1^{+0.9}_{-1.6})\times10^{52}$	$4.87\times10^{50}\uparrow$	$1.23^{+8.1}_{-0.26}\times10^{53}$	$1.93\times10^{51}\uparrow$	$1.54^{+2.7}_{-0.27}\times10^{53}$	$2.42\times10^{51}\uparrow$	—	–
130427A/2013cq	$(8.5\pm0.04)\times10^{53}$	$7.17\times10^{51}\uparrow$	$3.0^{+11.82}_{-1.19}\times10^{53}$	$2.54\times10^{51}\uparrow$	$1.5^{+1.19}_{-0.12}\times10^{54}$	$9.71\times10^{51}\uparrow$	$(6.39\pm0.7)\times10^{52}$	$13.2\uparrow$
130702A/2013dx	$(6.36\pm1.34)\times10^{50}$	$(1.9\pm1.64)\times10^{49}$	$1.92^{+5.23}_{-0.43}\times10^{52}$	$5.73^{+16.4}_{-2.49}\times10^{50}$	$1.98^{+4.24}_{-0.43}\times10^{52}$	$5.9^{+16.5}_{-5.15}\times10^{50}$	$(8.2\pm0.4)\times10^{51}$	6.71 ± 8.5
130831A/2013fu	$(4.6\pm0.2)\times10^{51}$	$7.06\times10^{48}\uparrow$	$5.27^{+11.59}_{1.16}\times10^{53}$	$8.08\times10^{50}\uparrow$	$5.32^{+11.64}_{-1.16}\times10^{53}$	$8.16\times10^{50}\uparrow$	$1.87^{+0.9}_{-0.62}\times10^{52}$	$4.18\uparrow$
140606B/iPTF14bfu	$(3.47\pm0.02)\times10^{51}$	$6.94\times10^{49}\uparrow$	$4.2\pm1.4\times10^{52}$	$8.4\times10^{50}\uparrow$	$4.5\pm1.4\times10^{52}$	$9.1\times10^{50}\uparrow$	$2\pm1\times10^{52}$	$4.31\uparrow$
161219B/2016jca	$(9.7\pm4.3)\times10^{49}$	$(2.36\pm1.05)\times10^{49}$	$1.6^{+3.52}_{-0.36}\times10^{50}$	$3.9^{+8.57}_{-0.85}\times10^{49}$	$2.57^{+3.95}_{-0.78}\times10^{50}$	$6.29^{+9.62}_{-2.69}\times10^{49}$	$(5.1\pm0.8)\times10^{52}$	0.12 ± 0.24

[a]The isotropic and jet-corrected prompt γ-ray emission energy of GRBs is calculated by using fluence and redshift extrapolated into 1-10,000 keV (rest frame) with a spectral model and a k-correction. The value of GRBs 011121 and 050525A are taken from Kan et al. 2010

[b]The isotropic and jet-corrected kinetic energy of GRBs measured from the afterglow flux during the normal decay phase.

[c]The isotropic and jet-corrected total energy of GRBs.

[d]The isotropic SN energy.

[e]The efficiency of GRB/SN events.

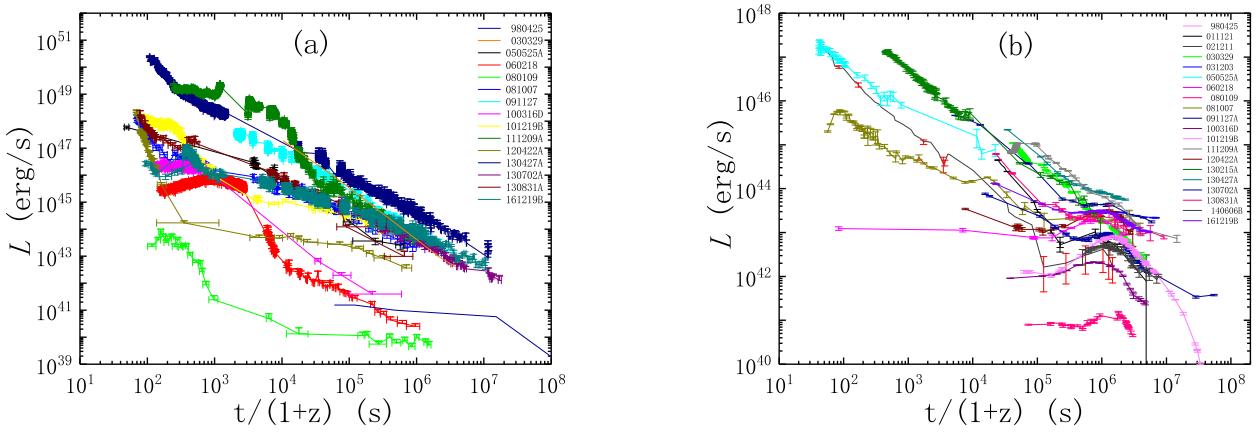

Fig. 1.— The X-ray (a) and optical (b) luminosity light curves of the GRB/SN systems in our sample in the rest frame.

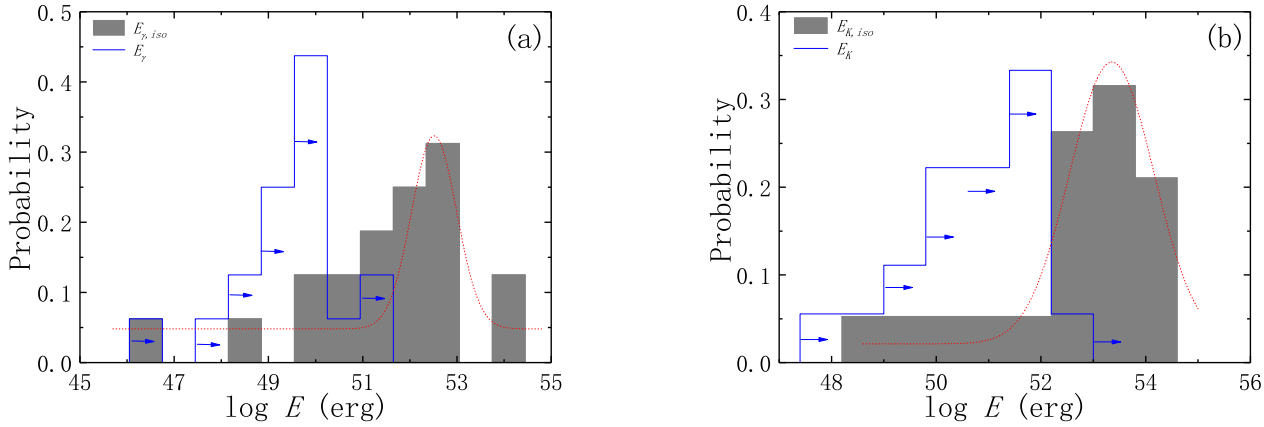

Fig. 2.— Distributions of the γ-ray energy (a) and kinetic energy (b) for the isotropic (gray-filled) and beaming-corrected values (blue solid line), respectively. Best-fit Gaussian profiles are denoted by red dotted curves. The arrows are ower limits on the energies after beaming correction.

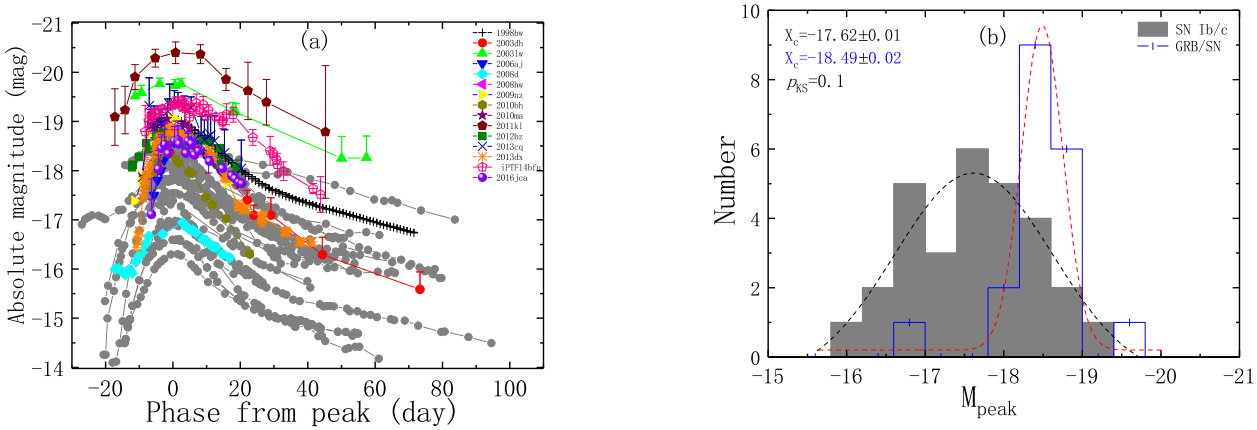

Fig. 3.— Comparison of the bolometric light curves (a) and peak magnitudes (b) of the GRB-associated SNe in our sample and other Type Ib/c SNe (gray). The data of other Type Ib/c SNe are taken from Lyman et al. (2016). The dashed lines of (b) are the best Gaussian fits.

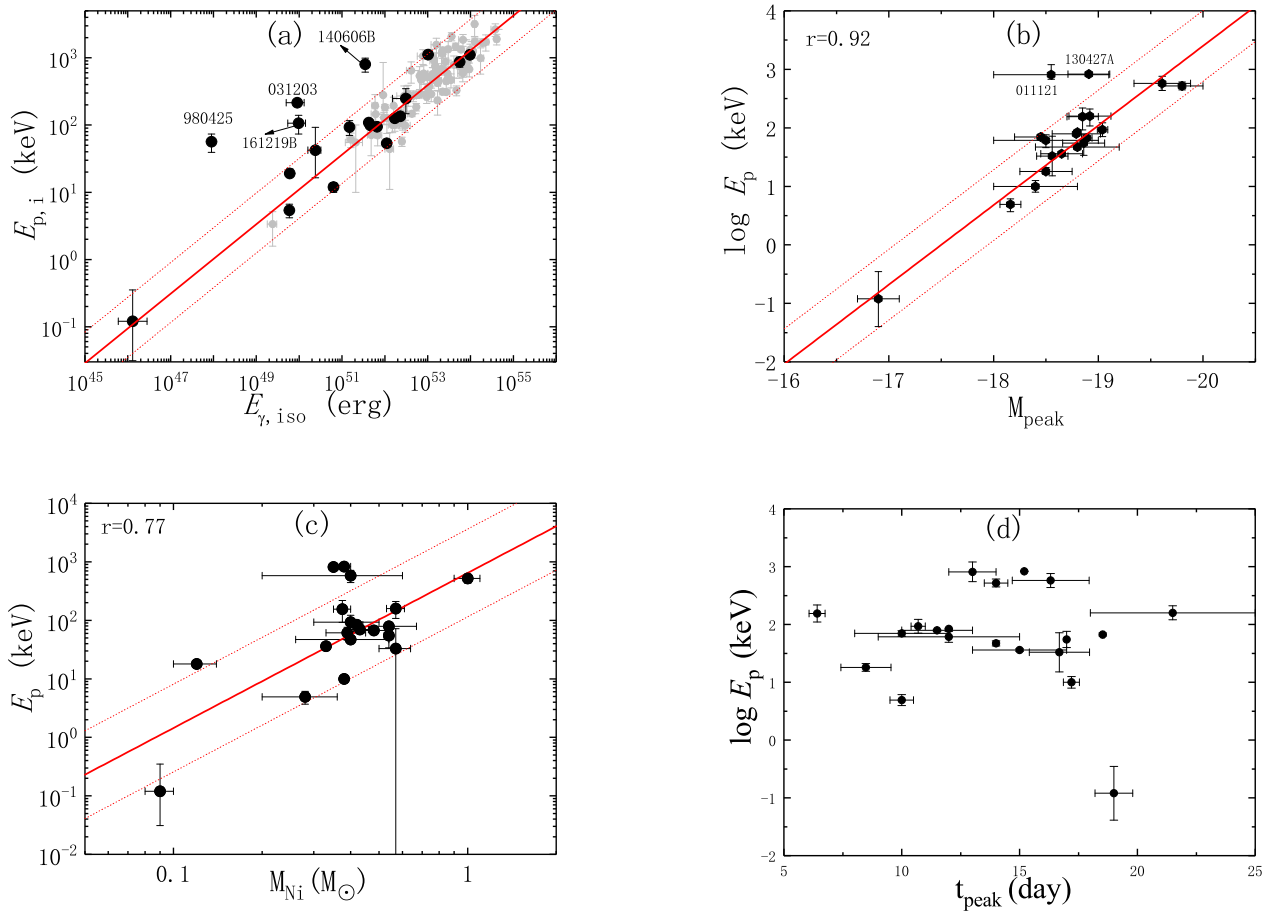

Fig. 4.— Spectral peak energy ($E_{\rm p}$) of GRBs as a function of $E_{\gamma,\rm iso}$ (a), $M_{\rm peak}$ (b), $t_{\rm peak}$ (c), and $M_{\rm Ni}$ (d). When a correlation exists, a solid line is drawn for the best power-law fit (for panel (a) the outliers are excluded). The dotted lines are the region of 2σ deviation.

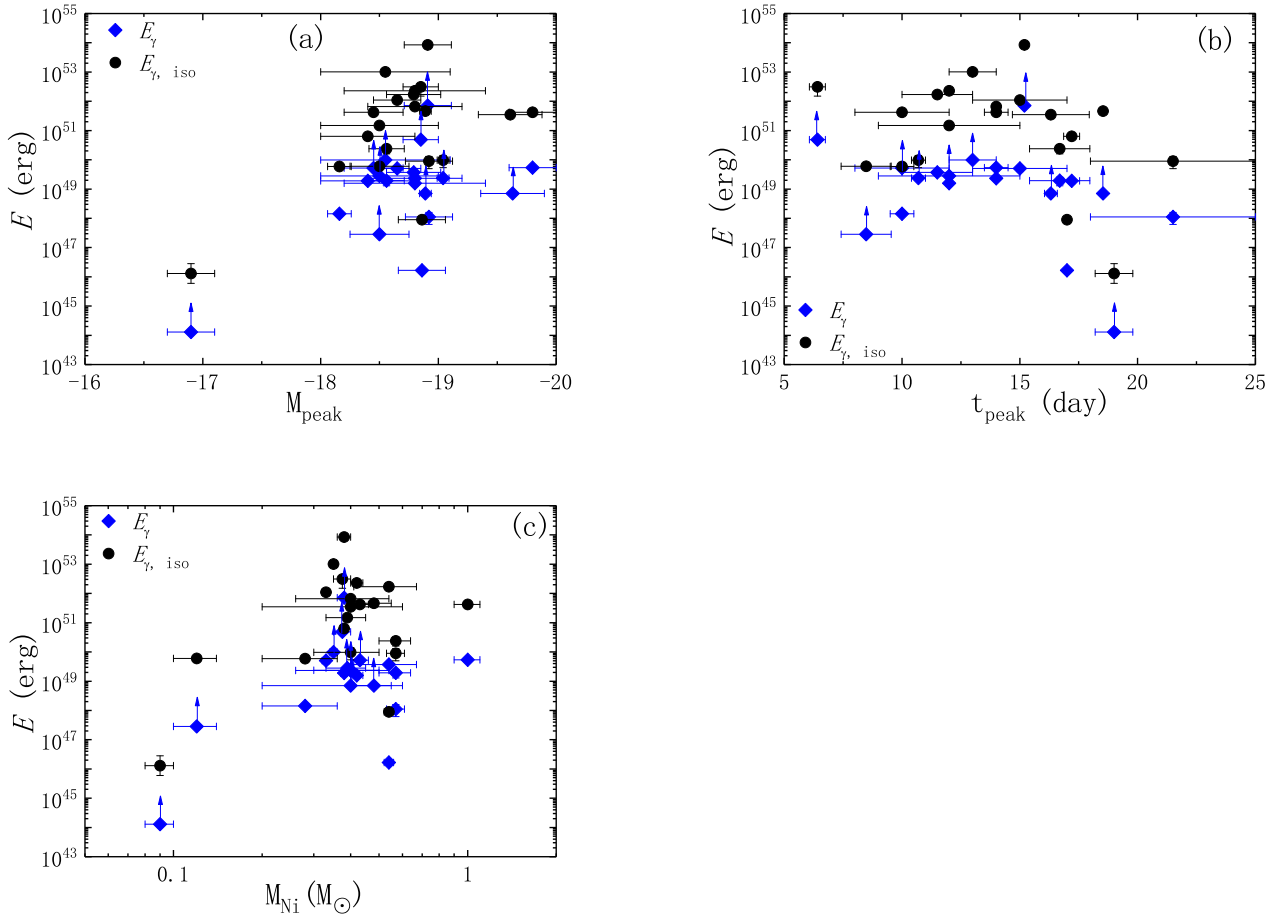

Fig. 5.— Isotropic (black dots) and beaming-corrected (blue diamonds) prompt γ-ray emission energies vs. $M_{\rm peak}$ (a), $t_{\rm peak}$ (b), and $M_{\rm Ni}$ (c). The blue arrows denote the lower limits of E_γ.

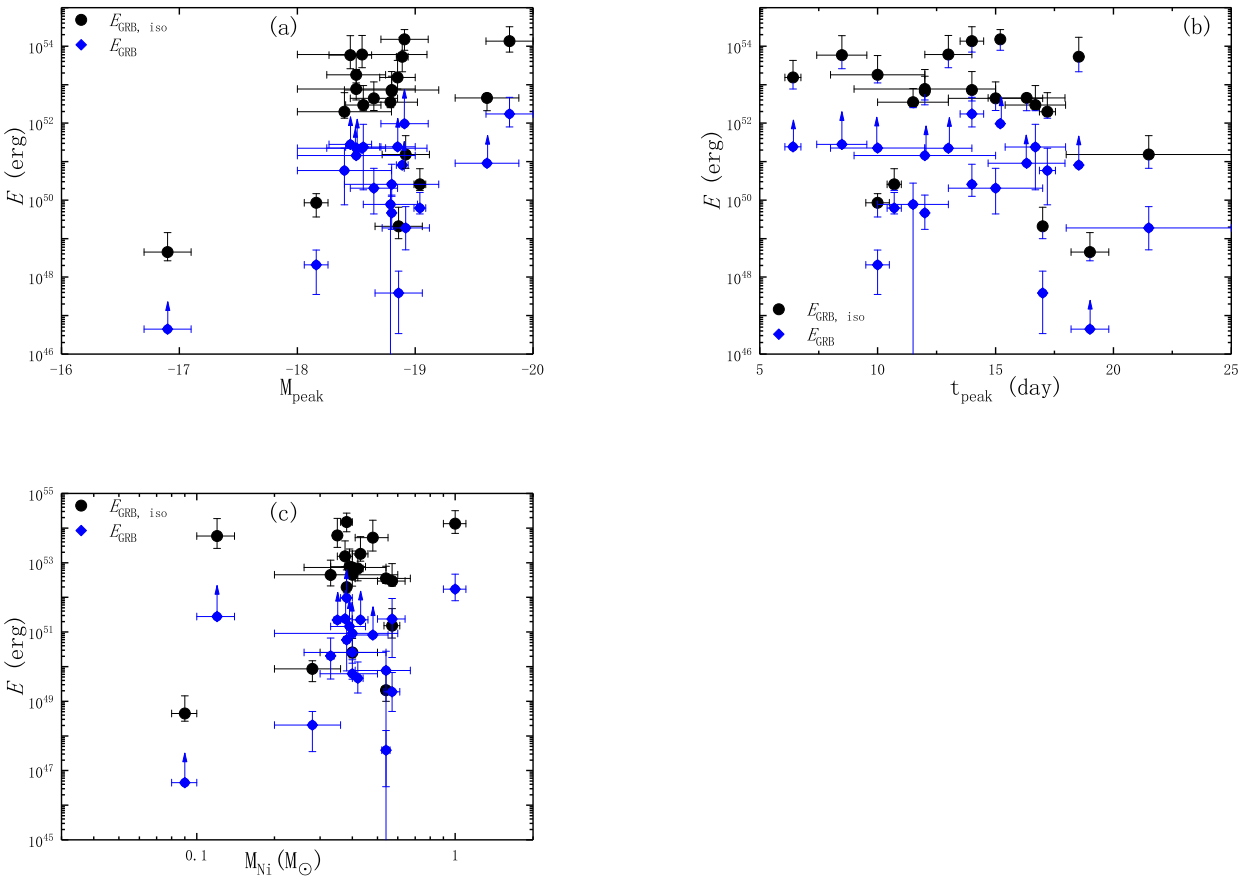

Fig. 6.— Similar to Figure 5, but for the total GRB energies.

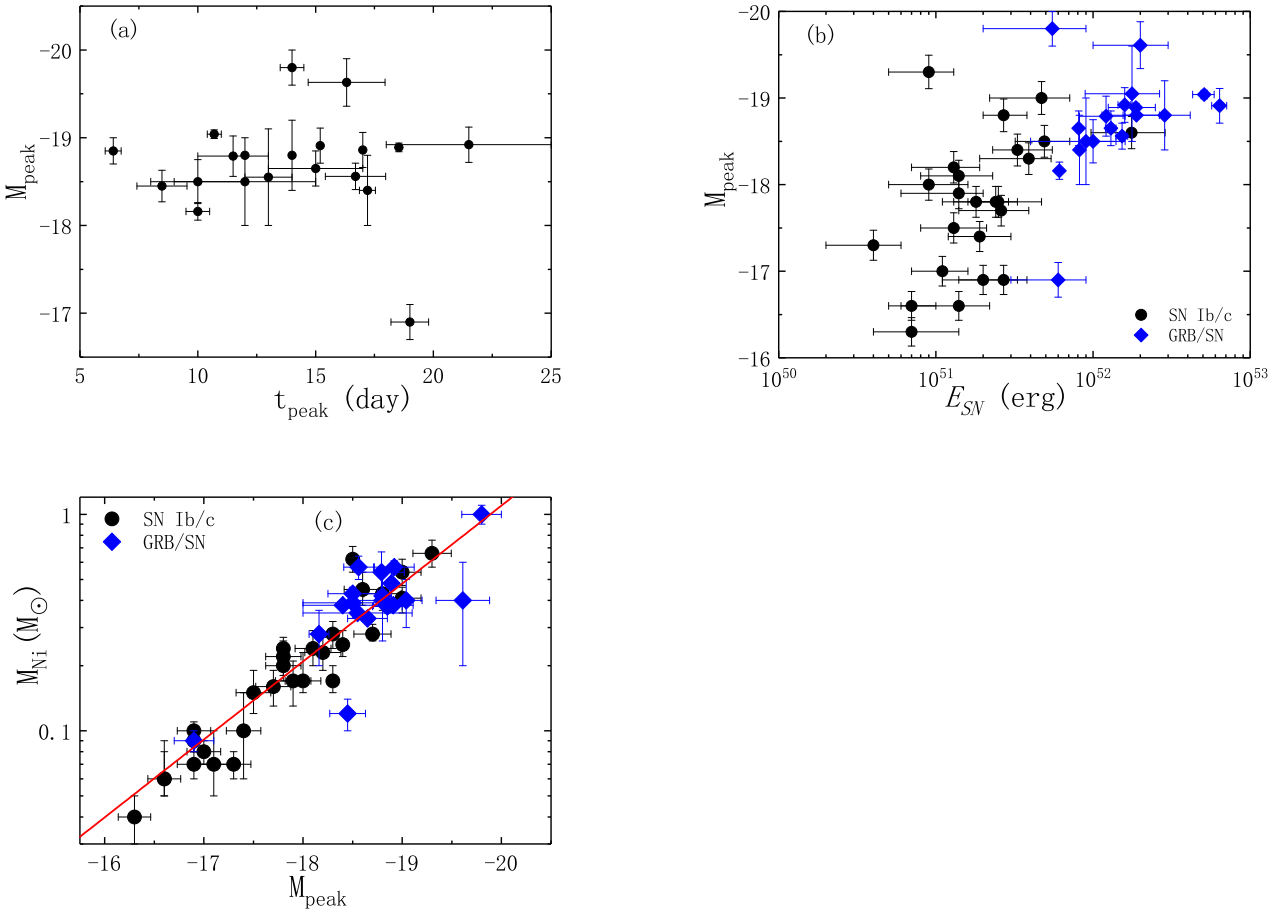

Fig. 7.— Peak magnitude ($M_{\rm peak}$) of SNe as a function of $t_{\rm peak}$ (a), $E_{\rm SN}$ (b), and $M_{\rm Ni}$ (c). The black dots and blue diamonds denote our sample and other Type Ib/c SNe without GRB association, respectively. The solid red line is the best power-law fit when an apparent correlation is seen.

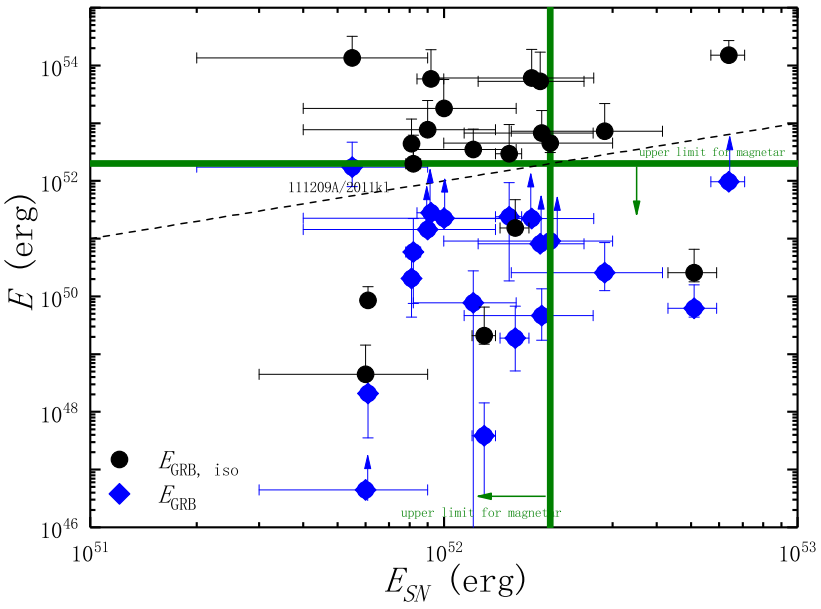

Fig. 8.— $E_{\rm GRB,iso}/E_{\rm GRB}$ vs. $E_{\rm SN}$ in our sample. The dashed line denotes the equality line. The vertical and horizontal lines are the upper limit of the magnetar energy budget.

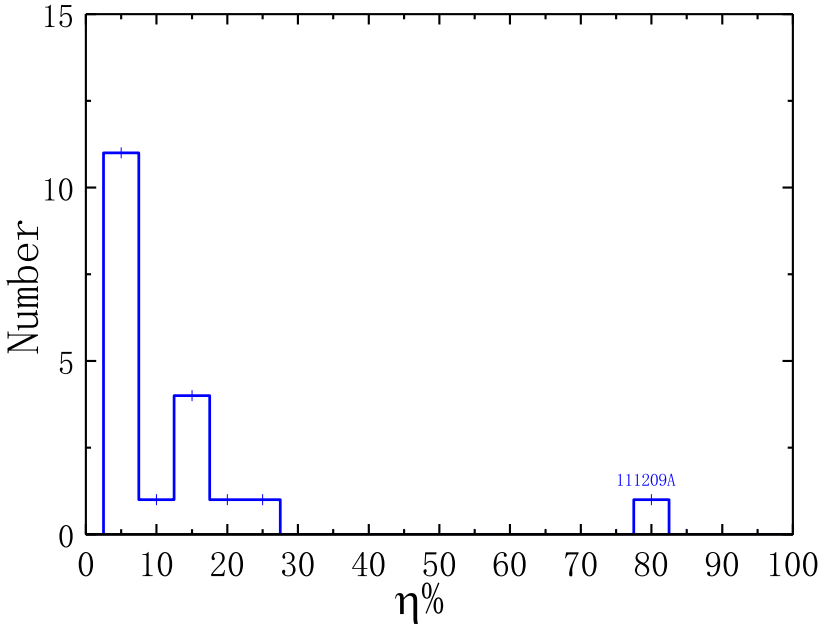

Fig. 9.— Distribution of η in our sample.

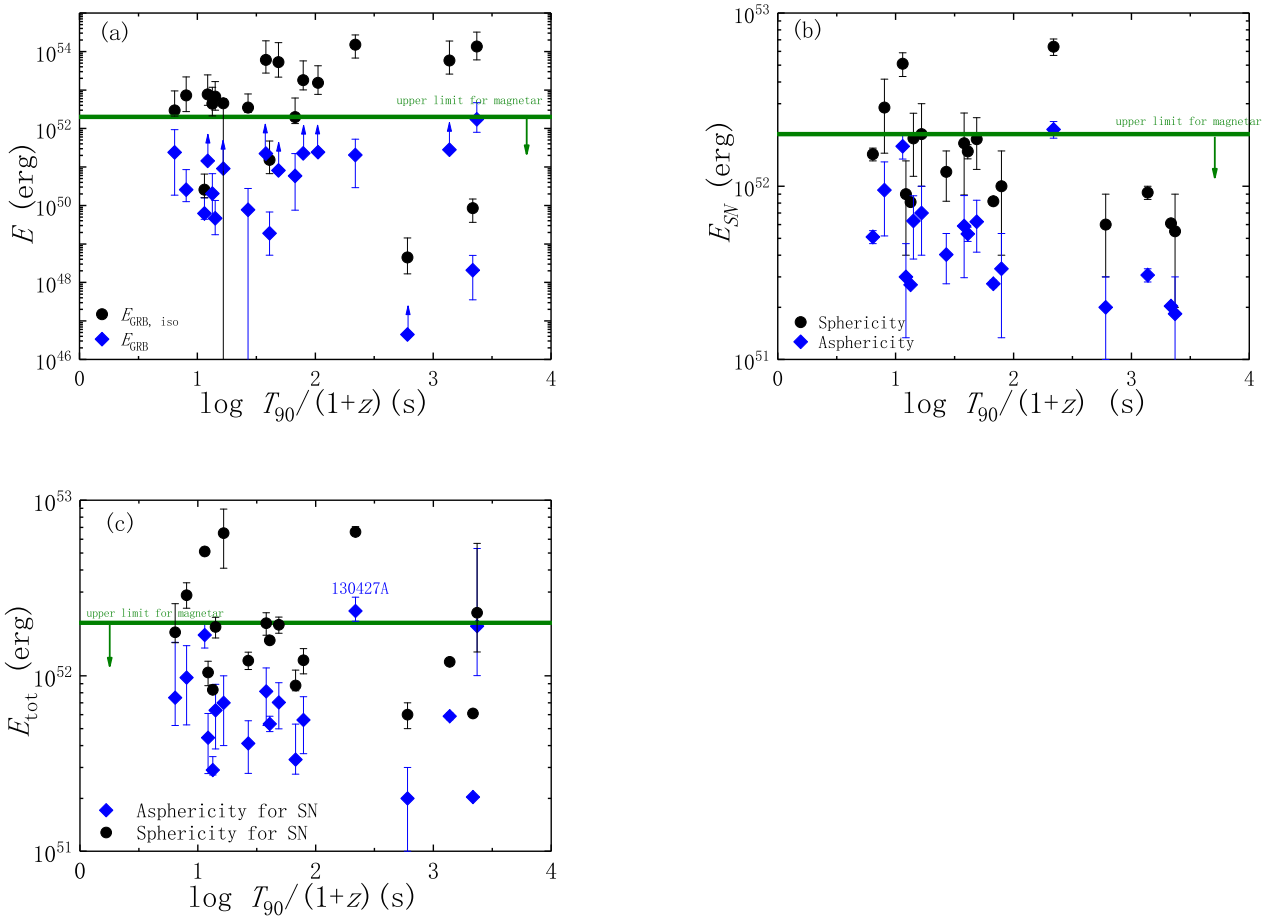

Fig. 10.— $E_{\rm GRB,iso}/E_{\rm GRB}$, $E_{\rm SN}$ and $E_{\rm tot}$ against GRB rest-frame duration. The horizontal line is the upper limit of the magnetar energy budget.

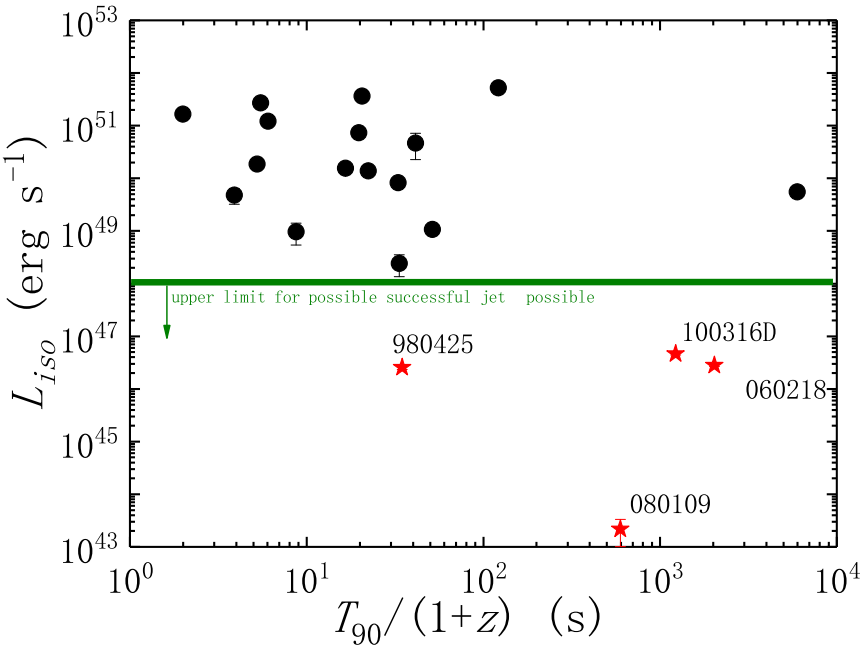

Fig. 11.— Isotropic luminosity of GRBs as a function of $T_{90}/(1+z)$ in our sample. Black dots denote the engine-driven GRBs, while red stars denote the possible shock-breakout GRBs suggested in the literature. The horizontal solid line (10^{48} erg s^{-1}) is a rough threshold above which successful jet breakout is possible (Zhang et al. 2012).